DRAGONWORX BIOMIMETIC TECHNOLOGIES

Technical Research Proposal

DragonSuit Apex

A Biomimetic Composite Wingsuit System:

Five-Layer Aerodynamic Stack and Wind Tunnel Validation Program

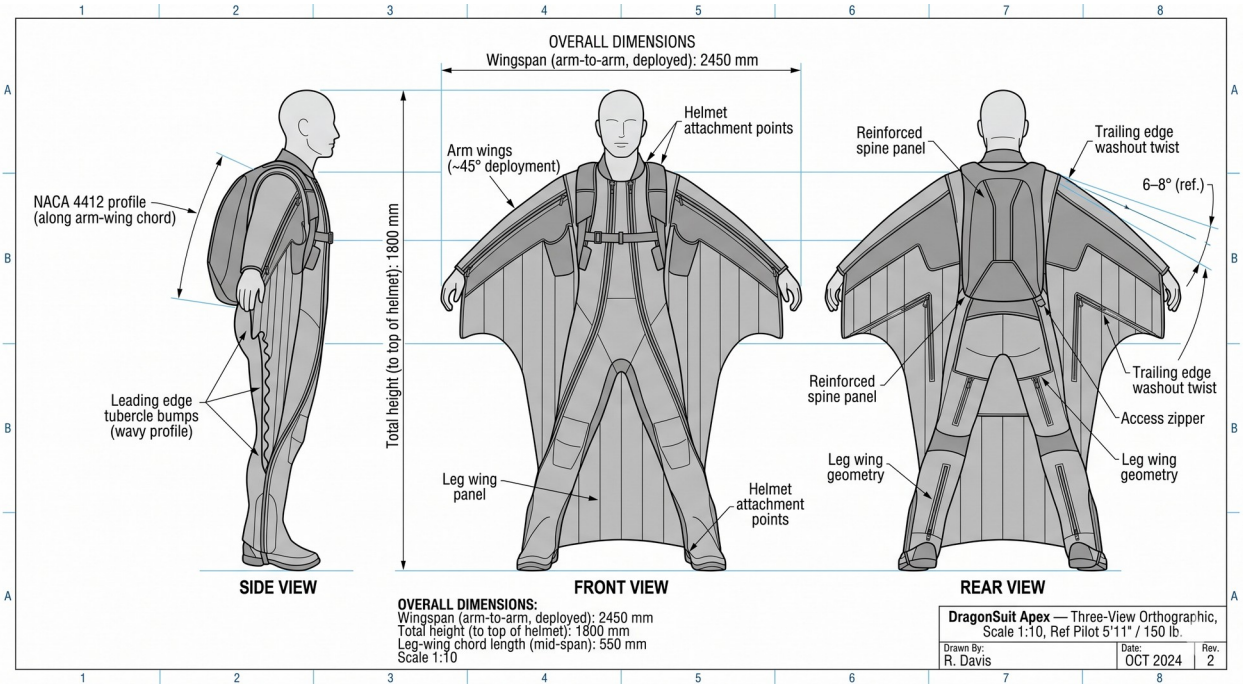

Figure 0.1 — DragonSuit Apex three-view orthographic. Wingspan 2,450 mm arm-to-arm (deployed). Reference pilot 5'11" / 150 lb. Scale 1:10.

Prepared for:

Aerodynamics Research Programs at Advanced Wind Tunnel Facilities
Department of Mechanical and Aerospace Engineering

Submitted by:

DragonWorx Biomimetic Technologies · Richardson, Texas
getdragons@dragonworx.bio · dragonworx.bio

May 2026 · Revision 1.0

Abstract

The DragonSuit Apex represents the first wingsuit system designed from aerospace materials science and fluid dynamics first principles rather than empirical iteration. Five discrete biomimetic technologies — each traceable to a validated biological mechanism — combine in a layered composite architecture to address the primary physical limitations that have constrained conventional wingsuit glide performance for three decades. These limitations include fabric billow under aerodynamic load (destroying wing geometry and L/D ratio), premature leading-edge stall, uncontrolled tip vortex-induced drag, laminar-to-turbulent boundary layer transition losses, and absence of passive washout under load.

The five-layer composite stack integrates: (1) laser-etched shark-denticle V-groove riblet film reducing skin friction drag 8–10% (TRL 6, production-validated in Speedo Fastskin and Lufthansa Technik programs); (2) a compliant flex wing membrane; (3) an auxetic metamaterial panel with re-entrant hexagonal lattice geometry that exploits negative Poisson's ratio mechanics to passively optimize chord camber under aerodynamic load with zero sensors or actuators; (4) a DiAPLEX shape-memory polymer (SMP) rib skeleton profiled to NACA 4412 cross-section that holds wing geometry under flight loads and resets to a flat stow profile at body temperature (37°C); and (5) a base compression layer. Leading-edge tubercles derived from humpback whale pectoral fin geometry (wavelength ~30% chord, amplitude ~5% chord) delay stall onset from 22° to approximately 28° angle of attack. An anisotropic washout weave at the wingtip — high-modulus spanwise fibers combined with oblique compliant twist fibers — induces 3–5° passive nose-down tip washout under aerodynamic load, suppressing tip stall through material mechanics alone.

CFD-based design targets project a glide ratio (L/D) of 5.0–6.0:1 for the full five-layer Apex stack. Reported glide ratios for high-performance competition wingsuits vary with measurement method and span roughly 2.5:1 to 3.5:1 for sustained glide; we adopt a conservative 3.0:1 reference and note that a meaningful share of in-flight wingsuit performance derives from active pilot control of body geometry, which a rigid test article cannot reproduce. The proposed program therefore measures a well-defined, repeatable aerodynamic quantity — the polar of a fixed geometry — rather than claiming equivalence to dynamic flight performance. Independent wind tunnel validation at a qualified aerodynamics research facility would provide the first aerodynamically rigorous characterization of this technology stack in an instrumented test environment. The proposed program is designed around the objections a wind tunnel aerodynamicist will raise first: Reynolds-number scaling and transfer to flight conditions, tunnel blockage at the large deployed span, simultaneous aeroelastic deformation measurement so that the as-loaded shape is known rather than assumed, shape-memory-polymer thermal-state control in an unoccupied model, and a full uncertainty budget on every reported coefficient (Section 6). This document describes the physics basis for each technology, defines the proposed wind tunnel experimental protocol, identifies the primary measurement objectives, and provides the engineering drawings necessary to construct a representative test article.

1. Introduction and Technical Motivation

1.1 The Empirical Ceiling of Conventional Wingsuit Design

Commercial wingsuits have achieved incremental glide ratio improvements over three decades through trial-and-error modification of fabric panel geometry, attachment point location, and cell inflation pressure. The current best-in-class L/D of approximately 2.8–3.0:1, reached by the highest-performing competitive suits, represents a plateau that has remained largely stationary for over a decade. The plateau exists not because the physics have been exhausted, but because the design methodology has been. No commercial wingsuit manufacturer has applied computational fluid dynamics to full-suit geometry, selected materials by aerodynamic functional requirement, or incorporated biomimetic surface science into the design architecture.

The DragonSuit program applies the design process in reverse order from conventional practice: physics requirements first, material selection second, suit geometry last. Each layer of the composite stack addresses a distinct and quantifiable aerodynamic or structural physics problem. The result is a system in which every material choice has a measurable aerodynamic justification.

1.2 Primary Physical Failure Modes in Conventional Wingsuits

Fabric billow and wing geometry collapse. Conventional wingsuit panels rely on internal air pressure and edge tension to maintain wing cross-section geometry. At speeds above approximately 50 m/s, dynamic pressure ($q = \frac{1}{2}\rho v^2$) exceeds the structural stiffness of the fabric panel and the wing billows — the upper surface rises away from the nominal airfoil profile, increasing effective camber non-uniformly and degrading both the suction peak on the upper surface and the pressure recovery toward the trailing edge. The net result is a significant reduction in L/D at speeds where the suit would otherwise operate most efficiently.

Laminar separation and premature stall. The arm-wing leading edge of a conventional wingsuit approximates a blunt cylinder — a geometry with no attention to controlled boundary layer attachment. At angles of attack above approximately 20–22°, the adverse pressure gradient on the suction surface triggers leading-edge separation, producing a stall that propagates spanwise and drives L/D below 1:1. This stall angle limit constrains the minimum glide speed and minimum deployment altitude for safe recovery.

Tip vortex-induced drag. The finite-span arm-wing generates a tip vortex whose rotational energy represents a direct transfer of kinetic energy out of the streamwise flow direction. The induced drag coefficient $C_{Di} = C_L^2/(\pi \cdot e \cdot AR)$ scales with the square of the lift coefficient and inversely with the wing aspect ratio and span efficiency factor e. For a wingsuit arm-wing with an estimated aspect ratio of approximately 3–4 and an unoptimized tip geometry, induced drag represents a substantial fraction of total drag, particularly at high angles of attack.

Skin friction drag. The woven nylon and spandex outer surfaces of conventional wingsuits present a hydraulically rough surface at flight Reynolds numbers ($Re \sim 1–3 \times 10^6$ at 40–60 m/s), promoting early boundary layer transition and elevated turbulent skin friction over the full chord length. The turbulent skin friction coefficient Cf is approximately 3–5× higher than the laminar value at equivalent Reynolds numbers, making the outer surface a significant and addressable drag source.

Absence of washout under load. Conventional wingsuits do not incorporate spanwise twist (washout), meaning the tip chord operates at the same angle of attack as the root. Under flight loads, fabric stretch at the tip can produce unintended twist in either direction, making stall behavior at the tip unpredictable and

potentially abrupt. A controlled, quantified, load-proportional nose-down tip washout would reduce the local angle of attack at the tip below the stall threshold even when the root approaches its limit.

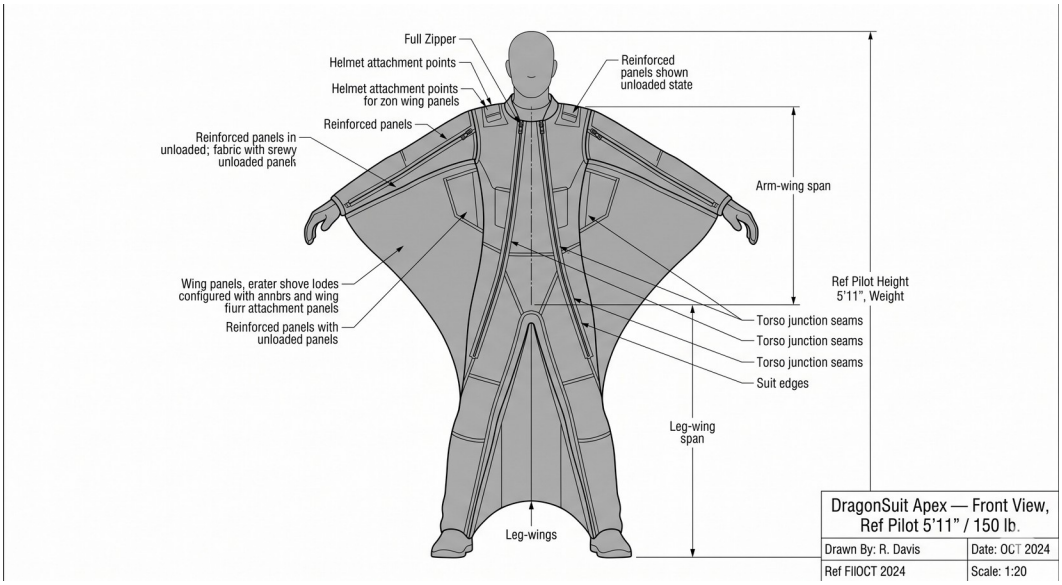

Figure 1.1 — DragonSuit Apex front-view orthographic. Arm wings at approximately 45° deployment. Leg-wing panel geometry and torso junction seams visible. Reference pilot 5'11" / 150 lb. Scale 1:20.

2. Five-Layer Composite Architecture

The DragonSuit Apex arm-wing and leg-wing panels incorporate five discrete functional layers. Each layer addresses one or more of the failure modes described in Section 1. The layers are not independent — they interact structurally and aerodynamically. Figure 2.1 illustrates the exploded assembly of the stack at a representative 30 cm × 30 cm panel section.

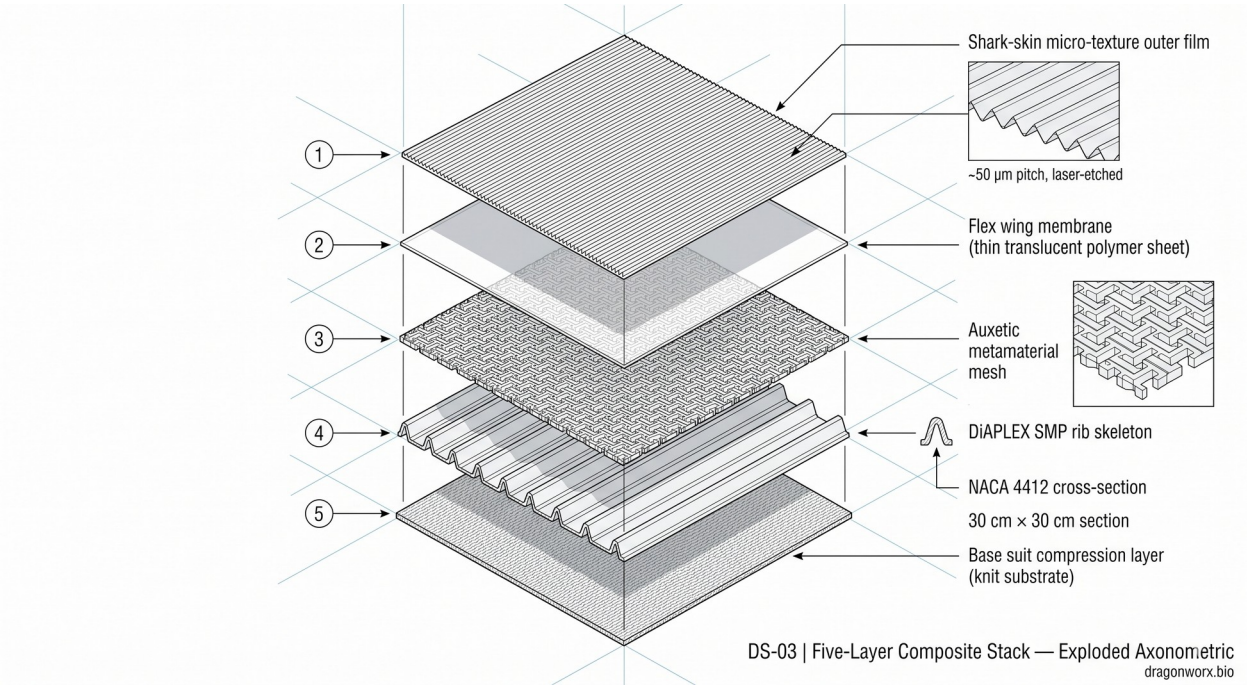

Figure 2.1 — Five-layer composite stack, exploded axonometric. From outer surface to body contact: (1) shark-skin riblet film, ~50 µm V-groove pitch, laser-etched; (2) flex wing membrane; (3) auxetic metamaterial mesh; (4) DiAPLEX SMP rib skeleton, NACA 4412 cross-section; (5) base compression layer.

2.1 Layer 1: Shark-Denticle Riblet Film (TRL 6)

The outermost surface layer consists of a laser-etched polymer film carrying parallel V-groove riblets oriented in the primary freestream direction. The riblet geometry — groove depth g ≈ 20 µm, ridge-to-ridge spacing s ≈ 50 µm — replicates the scale-averaged geometry of shortfin mako (Isurus oxyrinchus) denticles. The non-dimensionalized riblet spacing $s^+ = s \cdot u^*/\nu$ (where u^* is the friction velocity and ν is kinematic viscosity) targets $s^+ \approx 8–15$, the range established by Walsh (1982, 1990) and Bechert et al. (1997) as optimal for skin friction reduction in turbulent boundary layers at aeronautically relevant Reynolds numbers.

The mechanism operates by confining the quasi-streamwise vortices of the turbulent buffer layer between riblet ridges. The ridges reduce the contact area between high-speed outer-layer fluid and the wetted surface, decreasing the Reynolds shear stress contribution to skin friction. The peak drag reduction of 8–10% in turbulent skin friction coefficient Cf has been validated in production applications: Speedo Fastskin competitive swimwear (1996 Atlanta Olympics onward) and the Lufthansa Technik airfoil riblet film program for commercial transport fuselages. At wingsuit flight Reynolds numbers ($Re \approx 1–3 \times 10^6$) where the boundary layer transitions to turbulent well forward of the leading edge, the riblet film provides a uniform, quantifiable drag reduction across the full wetted area of the suit.

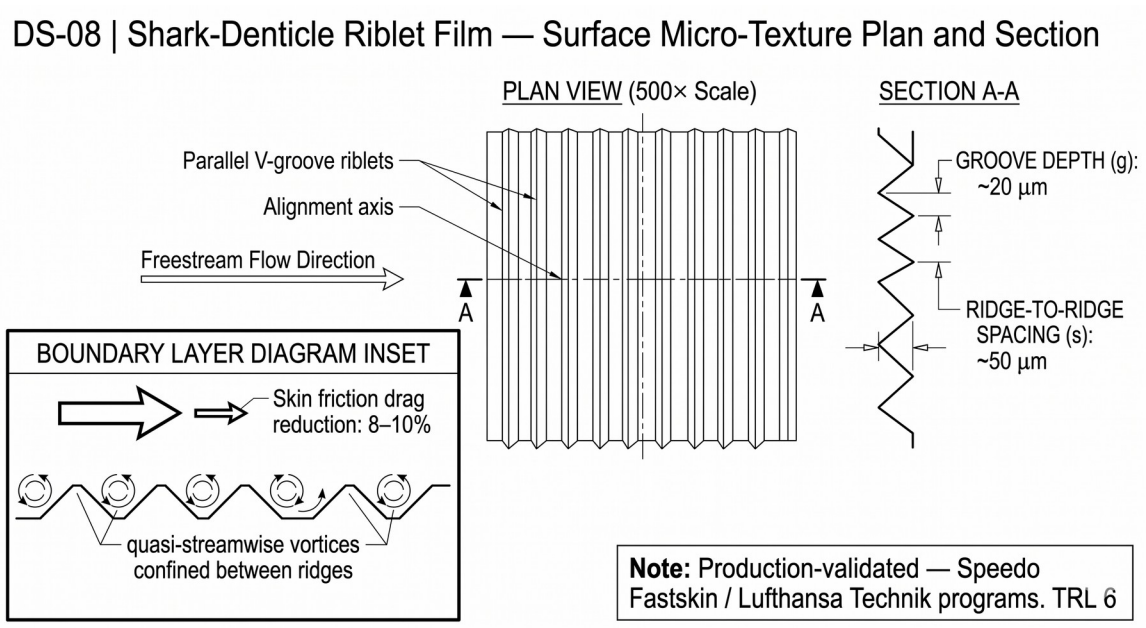

Figure 2.2 — Shark-denticle riblet film, plan view (500× scale) and Section A-A. V-groove depth g ≈ 20 µm, ridge-to-ridge spacing s ≈ 50 µm. Boundary layer inset: quasi-streamwise vortices confined between ridges reduce turbulent skin friction 8–10%. Production-validated. TRL 6.

2.2 Layer 2: Flex Wing Membrane

The second layer is a thin, compliant polymer membrane whose primary function is to transmit aerodynamic pressure loads from the outer riblet film to the structural layers below while accommodating the differential displacement required by the auxetic metamaterial panel in Layer 3. The membrane must satisfy two conflicting requirements simultaneously: sufficient stiffness to transmit pressure without local wrinkling or stress concentration, and sufficient compliance to permit the in-plane lateral expansion of the auxetic layer beneath it. Material selection for this layer represents an active design optimization target, with candidate materials including thermoplastic polyurethane (TPU) film and silicone-coated nylon.

2.3 Layer 3: Auxetic Metamaterial Panel — Passive Self-Cambering Wing

The center functional layer is the most aerodynamically consequential passive technology in the stack. The panel consists of a planar re-entrant hexagonal (bow-tie) lattice with a negative Poisson's ratio (NPR) — a so-called auxetic metamaterial. When a conventional material experiences in-plane tensile stress in one direction, it contracts in the orthogonal direction (positive Poisson's ratio, $\nu > 0$). The re-entrant lattice geometry inverts this behavior: the same tensile load causes the structure to expand in all in-plane directions simultaneously ($\nu < 0$).

The aerodynamic consequence is a passive, load-proportional change in wing geometry. Under aerodynamic pressure loading, the spanwise tension in the wing panel causes the auxetic layer to expand in the chordwise direction. This chordwise expansion, acting against the constraint of the leading and trailing edge attachment points, curves the chord into a higher-camber profile — a shape geometrically closer to the maximum-L/D NACA 4412 target. The wing effectively optimizes its own camber as a function of dynamic pressure, requiring no sensors, actuators, electronics, or active control loops.

The unit cell geometry for the DragonSuit implementation is a re-entrant hexagon with nominal strut length L = 10 mm, strut width t = 1.5 mm, and internal cell angle $\theta = 120°$. The center wing panel measures approximately 40 cm × 60 cm. At a typical flight dynamic pressure of $q = ½ \times 1.225 \times 50^2 \approx 1{,}530$ Pa, the

lateral expansion of the auxetic layer produces an estimated chordwise camber increase of 0.5–1.5% chord, shifting the effective profile from the unloaded flat state toward the 4% camber of the NACA 4412 target profile.

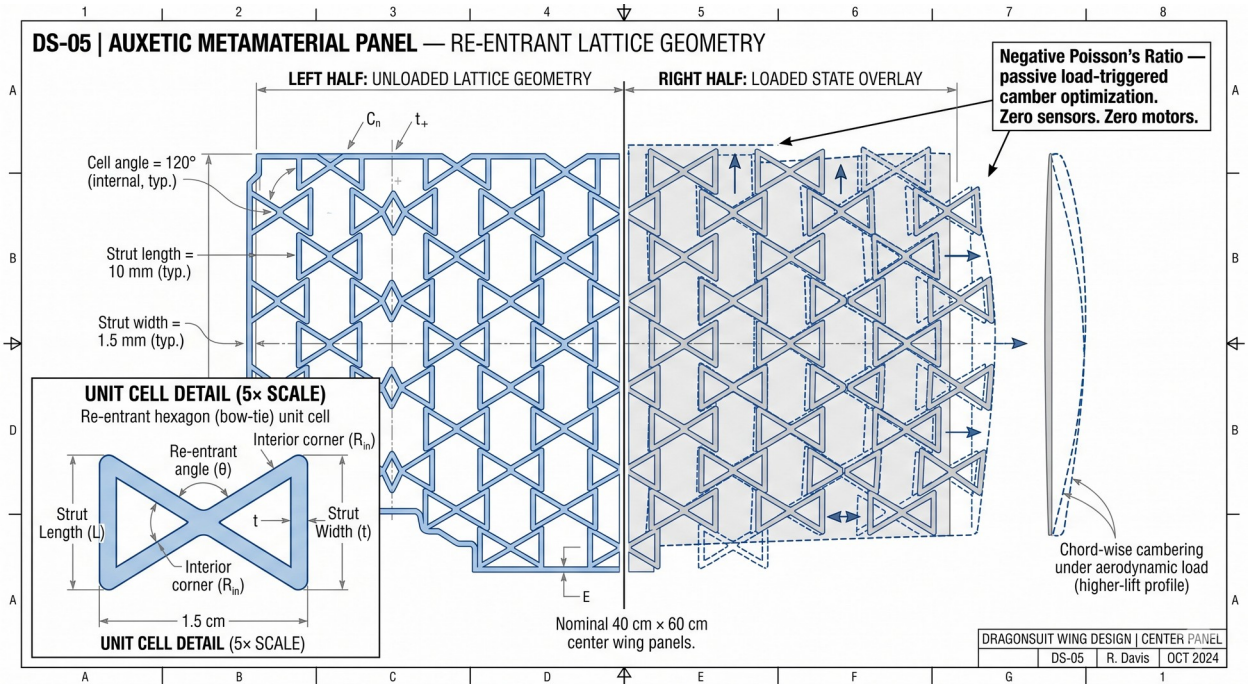

Figure 2.3 — Auxetic metamaterial panel DS-05. Left: unloaded re-entrant hexagonal lattice, strut L = 10 mm, strut width t = 1.5 mm, cell angle θ = 120°. Right: loaded state overlay (dashed) showing lateral expansion under aerodynamic load and chordwise cambering into higher-lift profile. Unit cell detail inset at 5× scale. Nominal panel 40 cm × 60 cm.

2.4 Layer 4: DiAPLEX Shape-Memory Polymer Rib Skeleton

The structural core of the wing panel is an array of spanwise ribs molded from DiAPLEX SMP (Mitsubishi Heavy Industries), a segmented polyurethane shape-memory polymer with a thermal transition temperature (Ttrans) close to 37°C — human body temperature. The ribs are precision-molded to the NACA 4412 cross-section: maximum camber 4% at 40% chord, maximum thickness 12% of chord. Nominal chord at mid-arm-span is approximately 350 mm, giving a maximum thickness of 42 mm.

Below Ttrans, DiAPLEX occupies its rigid, high-modulus glassy state. In this state the ribs maintain their molded NACA 4412 profile against aerodynamic pressure loads, preventing the fabric billow that degrades every conventional wingsuit's effective wing geometry. The bending stiffness EI of an SMP rib in the glassy state at 20°C is estimated at approximately 0.4–0.8 N·m² — sufficient to resist the bending moment imposed by distributed aerodynamic pressure of approximately 1,500–3,000 Pa over a representative rib tributary area.

At and above Ttrans (body contact or direct warming), the SMP transitions to its rubbery plateau state, reducing modulus by 2–3 orders of magnitude. In the rubbery state the ribs offer no shape resistance and the panel collapses to a flat, compact stow profile for donning, doffing, and packing. The transition is fully reversible and requires no mechanical intervention — the thermal cycle of body heat and ambient cooling drives the state change automatically on every use cycle.

This single technology — the SMP rib skeleton — accounts for the largest projected share of glide ratio improvement in the DragonSuit stack. The elimination of fabric billow restores the designed NACA 4412 geometry at the operating speeds where that geometry produces peak L/D.

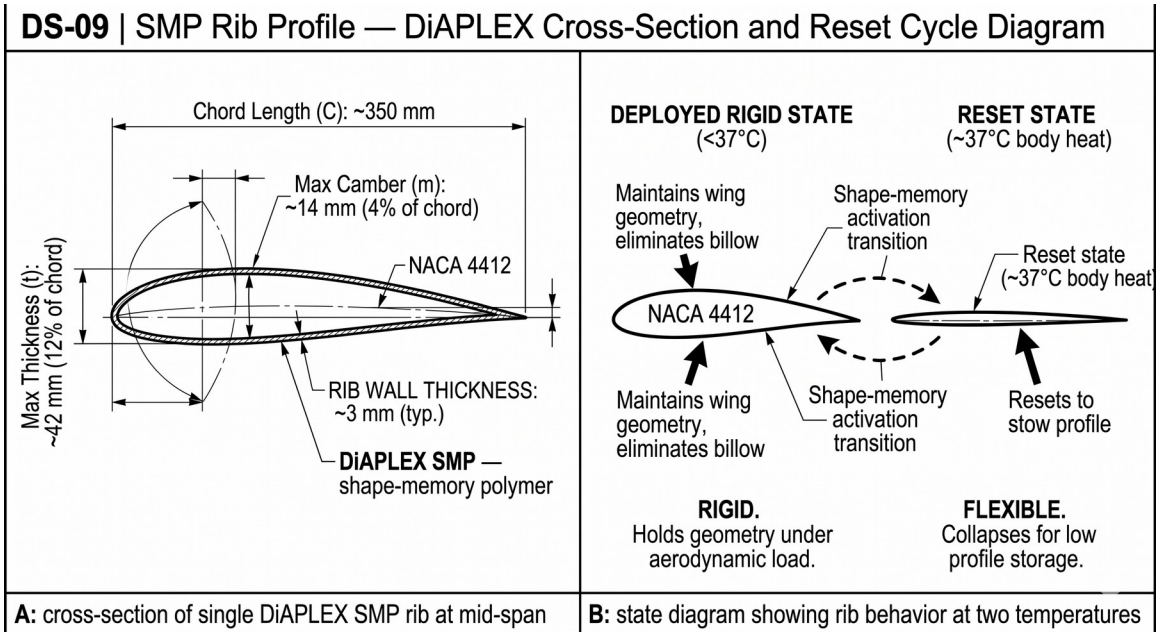

Figure 2.4 — DiAPLEX SMP rib profile (DS-09). Left: cross-section at mid-span. Chord C ≈ 350 mm, max camber 14 mm (4% C) at 40% C, max thickness 42 mm (12% C), rib wall thickness ~3 mm. Right: two-state thermal cycle diagram. Glassy state (<37°C): rigid, holds NACA 4412 geometry under aerodynamic load. Rubbery state (~37°C): flexible, collapses to flat stow profile.

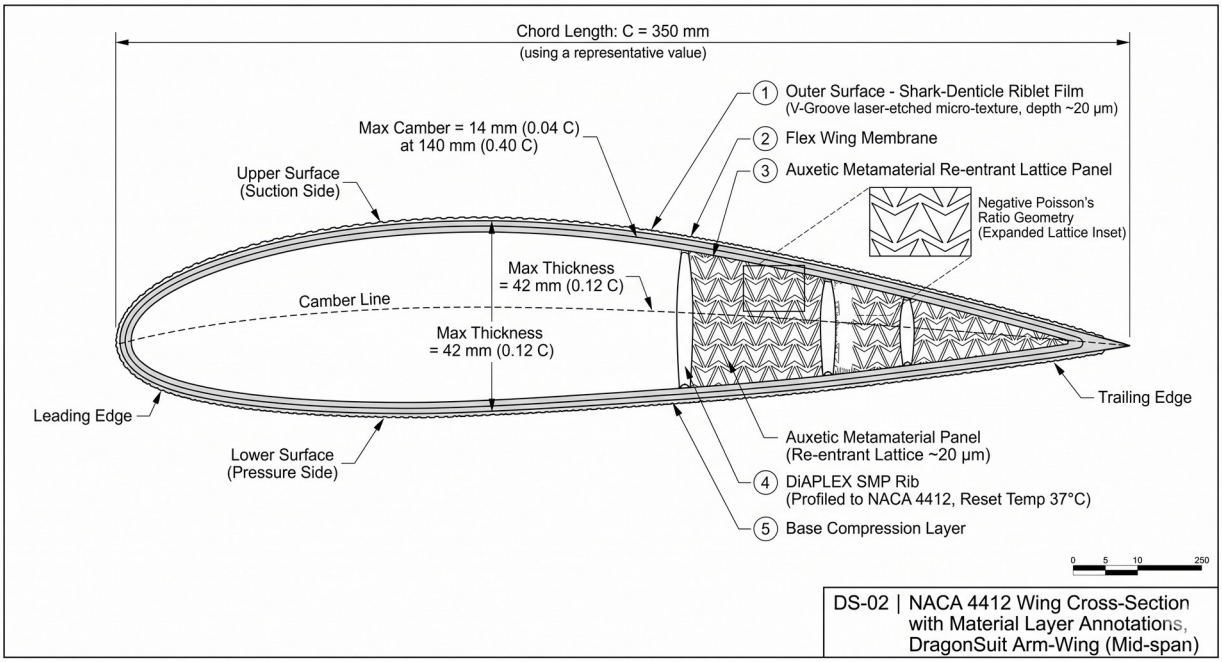

Figure 2.5 — NACA 4412 arm-wing cross-section with material layer annotations (DS-02). Chord C = 350 mm (representative). Upper surface (suction side), lower surface (pressure side), and camber line labeled. All five composite layers annotated at trailing-edge cutaway: (1) riblet film, (2) flex membrane, (3) auxetic lattice, (4) SMP rib, (5) base compression layer.

2.5 Layer 5: Base Compression Layer

The innermost layer is a stretch knit compression substrate that serves as the wearable base of the system, providing pilot comfort, moisture management, and a consistent attachment surface for the structural rib array above. The compression layer does not contribute aerodynamic function but provides the tensile preload that maintains panel planform geometry in the absence of aerodynamic loading — preventing the arm and leg wings from dragging or folding during low-speed maneuvering.

3. Biological Mechanism Technologies

3.1 Humpback Whale Tubercle Leading Edge (TRL 4)

Humpback whale (Megaptera novaeangliae) pectoral fins carry a series of rounded protuberances — called tubercles — along the leading edge. The spanwise wavelength of these tubercles is approximately 25–30% of the fin chord length, with a peak-to-trough amplitude of approximately 5% chord. Fish et al. (1995, 2011) demonstrated that the tubercle geometry delays stall onset by approximately 40% in angle of attack, reducing the stall angle from roughly 20° on a smooth leading edge to approximately 28° on a tubercle-modified profile.

The mechanism operates through controlled micro-turbulence injection. The sinusoidal leading-edge geometry divides the spanwise wing into discrete aerodynamic cells, each bounded by the troughs of adjacent tubercles. The troughs generate paired counter-rotating vortices that energize the boundary layer locally — maintaining attached flow into the adverse pressure gradient region at angles of attack that would cause global leading-edge separation on a smooth wing. The stall, when it occurs, propagates as discrete spanwise cell failures rather than as a single catastrophic leading-edge separation front, producing a progressive and recoverable degradation in lift coefficient rather than an abrupt stall break.

The DragonSuit implementation applies a precision-molded TPU strip to the arm-wing leading edge. The tubercle wavelength scales to approximately 30% of the 350 mm chord (105 mm wavelength) with amplitude of approximately 17 mm (5% chord). On the Apex SKU this strip is precision-molded to the full sinusoidal geometry. The Scout entry SKU uses a silk-screened surface approximation of the sinusoidal profile on a straight leading edge — providing some stall-delay benefit at significantly lower manufacturing cost.

The aerodynamic benefit in the DragonSuit context is a 6° extension of the operational angle-of-attack envelope (from 22° to 28°), directly translating to a reduction in minimum deployment altitude for safe recovery and an expansion of the low-speed maneuvering envelope for terrain proximity flight.

3.2 Peregrine Falcon Tip Slot — Auxetic Wingtip (TRL 3)

Peregrine falcons (Falco peregrinus) spread their primary feathers during high-angle-of-attack phases of flight — maneuvering and landing — creating spanwise slots between adjacent primaries at the wingtip. Each slot converts the rotational energy of the incipient tip vortex into a streamwise forward thrust vector, reducing induced drag by approximately 30% relative to an unslotted wing at equivalent CL (Tucker, 1993; Withers, 1981).

The DragonSuit implements this mechanism through the auxetic panel geometry at the wingtip zone — the lateral 20% of arm-wing span (~300 mm). Under aerodynamic load, the negative Poisson's ratio of the re-entrant lattice in this region causes the tip panel to expand spanwise, passively opening four discrete slot gaps of approximately 25 mm width at 25 mm spacing. The slots open proportionally to the local dynamic pressure — they are widest at the speeds where induced drag is highest and the benefit is greatest. No actuators, servo mechanisms, or control inputs drive the slot opening. The mechanism is entirely geometry- and load-driven.

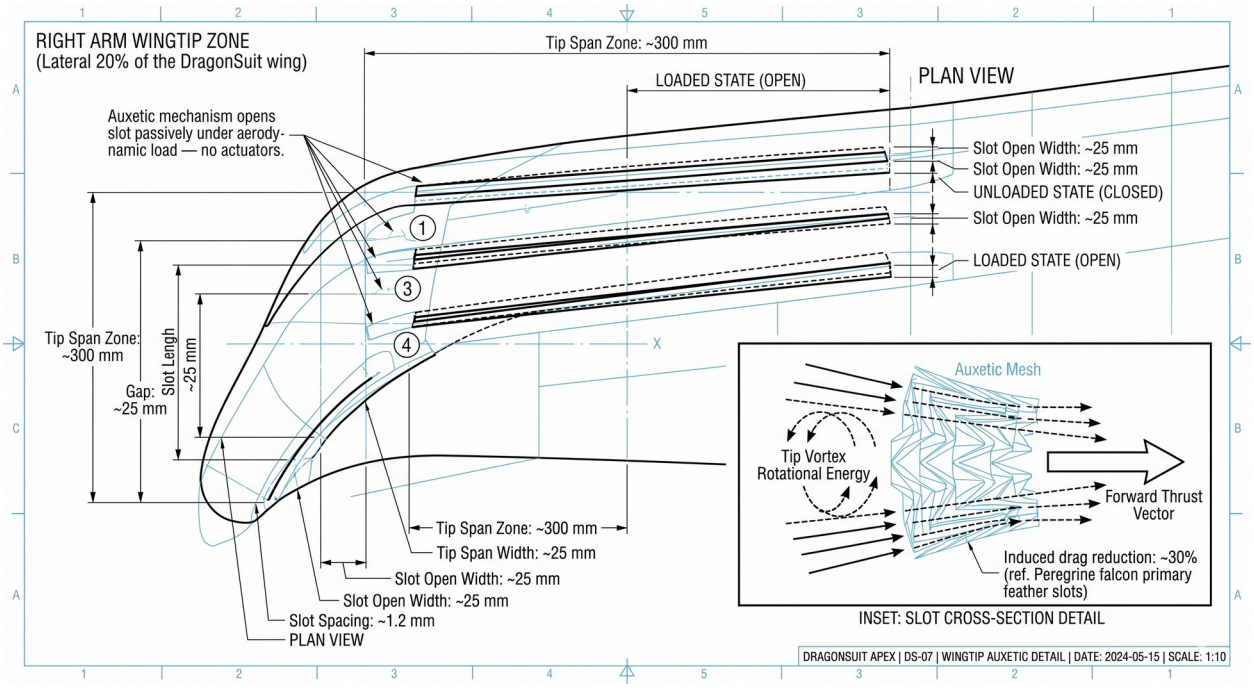

Figure 3.1 — Peregrine tip slot mechanism (DS-07). Right arm-wing tip zone, lateral 20% of span (~300 mm). Plan view: four slot gaps, unloaded (closed, solid lines) and loaded (open, dashed overlay). Slot open width ~25 mm, slot spacing ~25 mm. Inset: vortex energy recovery diagram — tip vortex rotational energy converted to forward thrust vector through slotted auxetic mesh. Induced drag reduction target: ~30%.

3.3 Anisotropic Washout Weave (TRL 4–5)

Geometric washout — a decrease in angle of attack from wing root to tip — is a standard technique in fixed-wing aircraft design to ensure that the wing root stalls before the tip, preserving aileron effectiveness and producing a recoverable stall progression. In conventional wingsuits no washout mechanism exists; the entire span operates at a nominally uniform angle of attack, with tip geometry determined by fabric stretch that is variable and uncontrolled.

The anisotropic washout weave addresses this by encoding passive twist behavior directly into the fiber architecture of the wing panel. High-modulus fibers oriented spanwise (parallel to the span axis) carry the primary aerodynamic loads in the spanwise bending mode. Compliant fibers oriented at an oblique angle to the chord axis provide the principal stiffness in the twist degree of freedom. Because these two fiber families have substantially different elastic moduli, the wing panel exhibits an anisotropic stiffness matrix: it is stiff in spanwise bending and compliant in twist.

Under distributed aerodynamic loading, the compliance in twist allows the tip region to rotate nose-down by 3–5° relative to the root — a passive washout that scales proportionally with the lift force and thus with the dynamic pressure. At the flight speeds and angles of attack where stall risk is highest (high q, high AoA), the washout is also greatest, providing the maximum stall protection when it is most needed. The mechanism introduces no added mass, no mechanical parts, and no power requirement. It is entirely encoded in the fiber orientation schedule of the weave.

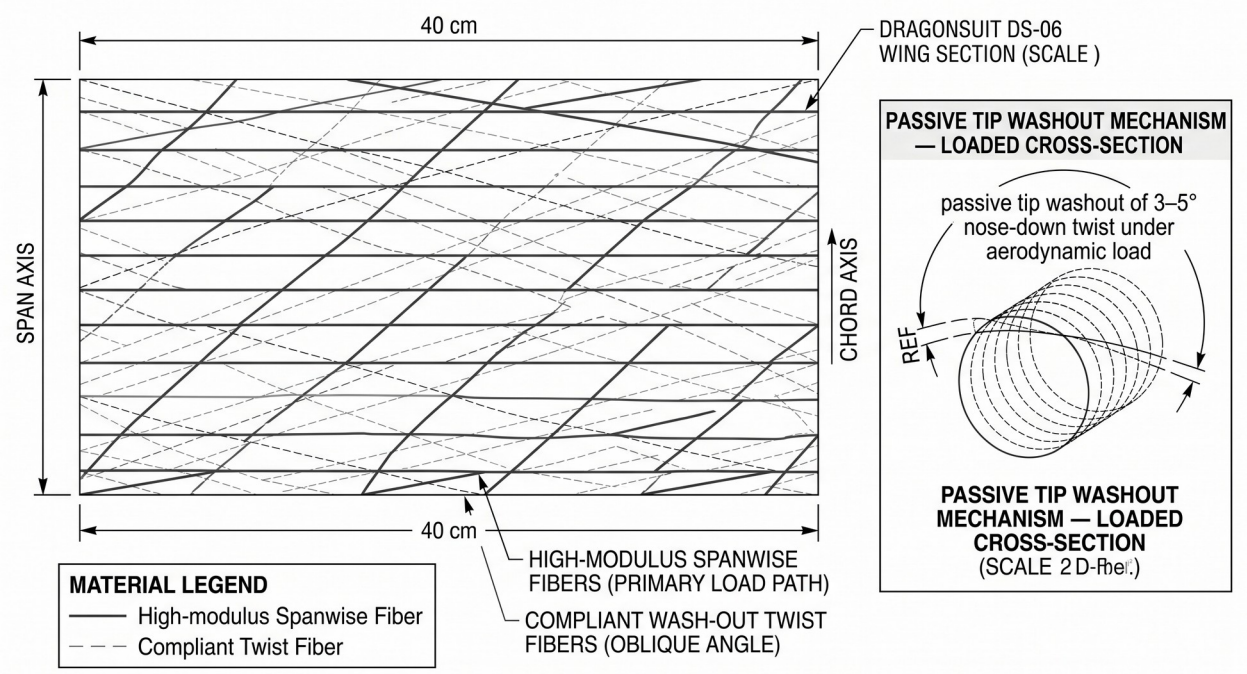

Figure 3.2 — Anisotropic washout weave (DS-06). 40 cm × 40 cm panel section. Primary spanwise load-path fibers (solid lines, parallel to span axis) combined with compliant oblique twist fibers (dashed lines). Inset: loaded cross-section showing passive tip washout of 3–5° nose-down under aerodynamic load. No mechanical parts. Behavior encoded entirely in fiber orientation schedule.

4. Performance Projections and Design Targets

4.1 Glide Ratio Analysis

The projected glide ratio improvement results from the additive but non-linear interaction of the five technology layers. The dominant contributors to L/D improvement are estimated individually below, with the understanding that aerodynamic interactions between layers — particularly between the SMP rib geometry maintenance and the auxetic camber optimization — will modulate the individual contributions.

Technology	Primary Mechanism	Isolated ΔL/D	TRL	Validation Basis
SMP Rib Skeleton	Eliminates fabric billow; maintains NACA 4412 geometry under load	Largest individual contributor — est. +0.8 to +1.5 L/D	TRL 4	DiAPLEX material properties; CFD geometry comparison
Auxetic Self-Cambering	Load-proportional camber optimization toward NACA 4412 peak	+0.3 to +0.7 L/D at design q	TRL 4	NPR theory; published auxetic aerospace literature
Tubercle Leading Edge	Stall delay 22° → 28° AoA; expands usable L/D range	+0.2 to +0.5 at high AoA	TRL 4	Fish et al. 1995, 2011; WT data on tubercle profiles
Shark Riblet Film	Reduces turbulent skin friction drag 8–10%	+0.1 to +0.2 (drag reduction)	TRL 6	Bechert et al. 1997; Speedo / LHT programs
Tip Slot + Washout	Reduces induced drag ~30% at tip; prevents tip stall	+0.1 to +0.3 at high CL	TRL 3–5	Tucker 1993; classical washout theory

The per-technology contributions in Table 4.1 are reported as isolated directional estimates, not as terms in a linear superposition. Lift and drag do not decompose additively across interacting mechanisms — the auxetic camber response, the SMP-maintained profile, the tubercle stall behavior, and the tip washout are aerodynamically coupled, and the integrated polar must be measured rather than summed. The values are presented to indicate the relative magnitude and direction of each mechanism's expected effect and to define what the Configuration C isolation tests must resolve. With these caveats, the integrated CFD model projects a full-stack L/D in the range of 5.0–6.0:1. We state plainly that this projection carries substantial uncertainty until measured: the purpose of the proposed program is precisely to determine whether the coupled system realizes the gain the component literature suggests, or whether destructive interactions erode it.

Figure 4.1 presents the L/D vs. angle of attack comparison between the conventional wingsuit baseline and the DragonSuit Apex design target. The most significant features are the elevated L/D peak (5.0–5.5:1 vs. 2.8–3.0:1), the extended stall-delay region between 22° and 28° AoA attributable to tubercle geometry, and the more gradual post-stall degradation enabled by the washout weave and slot mechanism.

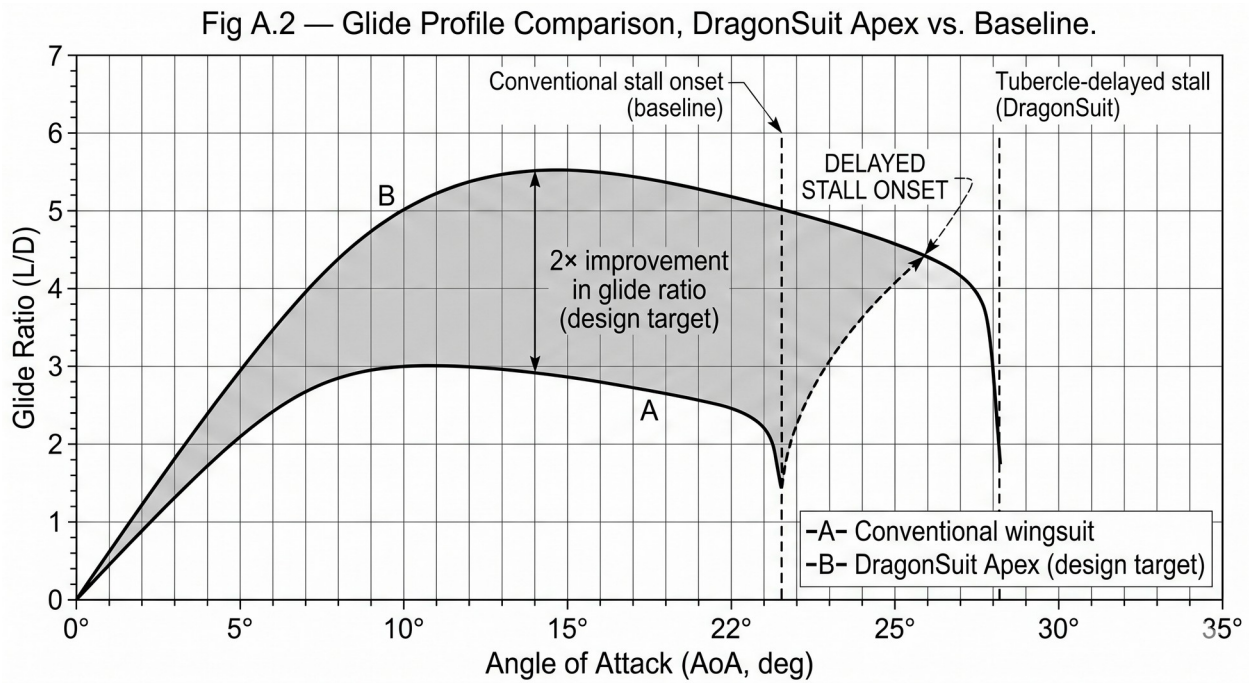

Figure 4.1 — Glide ratio comparison (DS-10 / Fig A.2). Curve A: conventional wingsuit baseline, peak L/D ≈ 2.8–3.0 at ~12° AoA, stall at ~22°. Curve B: DragonSuit Apex design target, peak L/D ≈ 5.5 at ~13° AoA, stall delayed to ~28°. Shaded region: 2× improvement envelope. All figures are CFD-based design targets pending wind tunnel validation.

4.2 Minimum Deployment Altitude

The practical safety benefit of an extended stall envelope is a reduction in the minimum altitude at which a wingsuit pilot can safely deploy a parachute following a controlled glide. Deployment altitude depends on the minimum airspeed at which the suit produces sufficient lift to maintain a stable, manageable glide angle during the deceleration phase of canopy opening. A higher stall angle of attack — achieved here by 6° through tubercle geometry — directly permits a lower minimum speed and thus a lower critical altitude. The DragonSuit design target of a 51% reduction in minimum deployment altitude relative to best-in-class derives from this relationship.

4.3 Product Line Performance Envelope

SKU	Price	Glide Ratio	Min Altitude	Key Technology	Market
DragonSuit Scout	$279–$349	3.8–4.5:1	~120 ft	EVA foam ribs + TPU tubercle strip	Consumer / Entry
DragonSuit Apex	$10K–$18K	5.0–6.0:1	~90 ft	Full 5-layer SMP/auxetic stack	Elite Pilots
DragonSuit Apex-M	$28K–$45K	5.0–6.0:1	<90 ft	Apex + helicoidal CFRP armor + MOLLE	Military / SOF
DragonSuit Apex-SAR	$18K–$24K	5.0–6.0:1	~90 ft	Apex + beacon integration + high-vis	SAR / Government

All glide ratio and altitude figures are design targets based on CFD simulation and published literature for individual component technologies. Wind tunnel validation constitutes the primary near-term experimental program for these projections.

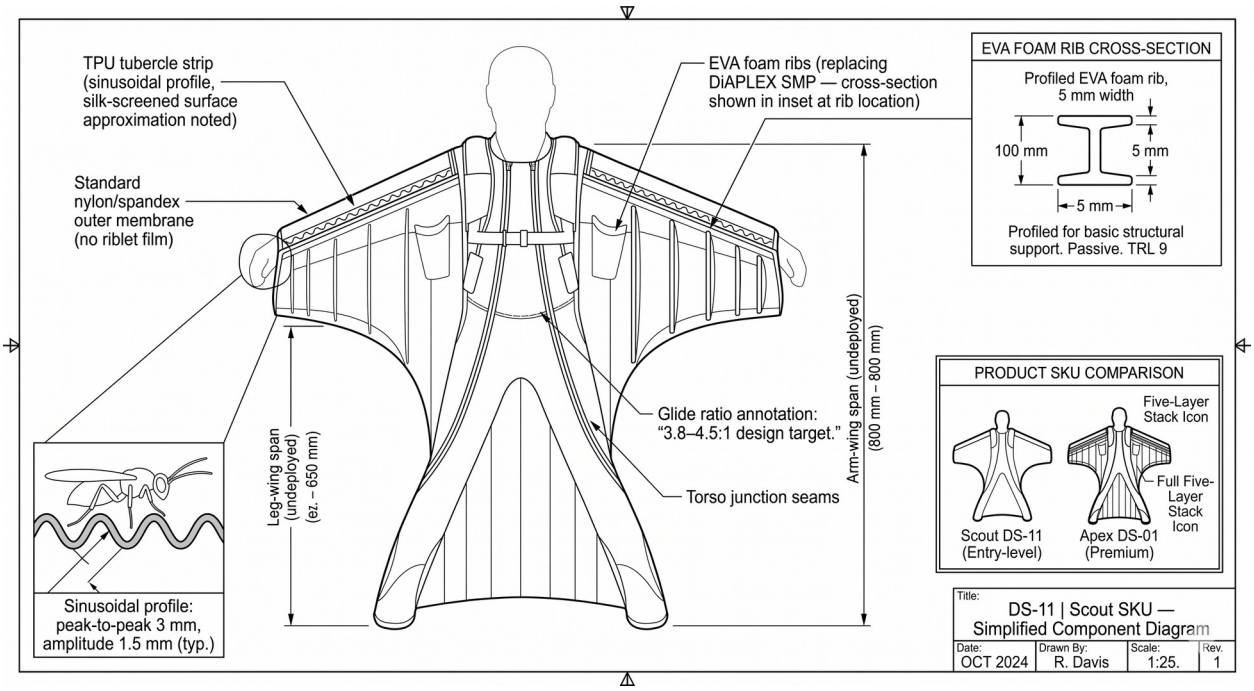

Figure 4.2 — DragonSuit Scout simplified component diagram (DS-11). Entry-level consumer SKU. EVA foam ribs (100 mm width, 5 mm wall, profiled for structural support) replace DiAPLEX SMP. TPU tubercle strip with sinusoidal profile (peak-to-peak 3 mm, amplitude 1.5 mm) retained at leading edge. No riblet film. Glide ratio design target: 3.8–4.5:1. SKU comparison inset: Scout vs. Apex five-layer stack.

5. Proposed Wind Tunnel Validation Program

5.1 Objectives

The primary objective of the proposed wind tunnel program is the experimental validation of the L/D improvement projected by CFD analysis for the DragonSuit Apex composite stack. Secondary objectives include characterization of stall onset angle as a function of leading-edge tubercle geometry, measurement of skin friction drag reduction attributable to the riblet film, and characterization of the auxetic panel's camber response as a function of dynamic pressure.

The program would produce the first aerodynamically rigorous, instrumented experimental characterization of a wearable wingsuit system in a controlled test environment — a dataset with value both to the DragonWorx development program and to the broader academic literature on biomimetic aerodynamic systems.

5.2 Test Article Configuration

Three test configurations are proposed for the wind tunnel program:

Configuration A — Isolated Arm-Wing Panel. A representative 350 mm chord × 600 mm span arm-wing section, full five-layer stack, mounted on a two-component force balance. This configuration isolates the aerodynamic contribution of the composite stack from body-wake interactions and permits direct comparison with a clean-sheet NACA 4412 baseline.

Configuration B — Full-Suit Mannequin. A rigid mannequin (5'11" / 150 lb reference pilot, per the dimensioned drawings) with deployed arm and leg wings in the DragonSuit Apex configuration, mounted on a six-component sting balance. This configuration captures body-wing interference effects, leg-wing contribution to total lift, and realistic planform efficiency.

Configuration C — Technology Isolation. Configuration A repeated with individual layers removed or substituted (plain membrane for riblet film; solid foam panel for auxetic layer; straight leading edge for tubercle strip) to isolate the individual contribution of each technology to the total L/D improvement. This produces a technology contribution matrix directly comparable to the projections in Table 4.1.

5.3 Test Conditions

Parameter	Value	Basis
Freestream velocity range	30–80 m/s (108–288 km/h)	Typical wingsuit flight envelope: terminal velocity ~50–60 m/s
Reynolds number range	$Re \approx 7\times10^5 – 2\times10^6$ (chord-based)	$Re = V\cdot c/\nu$, c = 350 mm, $\nu = 1.5\times10^{-5}$ m²/s
Angle of attack sweep	0° to 35° in 1° increments	Full pre-stall and post-stall characterization
Sideslip angle	0°, ±5°, ±10°	Assess asymmetric loading; yaw stability
Turbulence intensity	<0.1% (clean tunnel)	Isolate geometry effects from freestream turbulence
Measurement outputs	CL, CD, CM, Cp distribution, tuft/PIV flow visualization	Full polar + surface pressure distribution

5.3a Reynolds-Number Scaling and Test-Article Fidelity

The single greatest threat to the validity of this program is Reynolds-number mismatch. Two of the five technologies are explicitly Reynolds-sensitive. The riblet drag-reduction mechanism depends on the viscous-scaled rib spacing $s^+ = s \cdot u_\tau / \nu$, where u_τ is the friction velocity; the optimal $s^+ \approx 8–15$ band is fixed in wall units, so the physical rib geometry that is optimal at test Reynolds number differs from the geometry optimal at flight Reynolds number. The tubercle stall-delay mechanism is likewise Re-dependent (Hansen et al. 2011; Custodio 2007), with the magnitude of the delay varying across the transitional regime. A test conducted at a Reynolds number far below flight would therefore mischaracterize both effects.

We propose three mitigations, to be finalized with the host facility. First, the chord-based test Reynolds number range ($Re \approx 7\times10^5–2\times10^6$) is selected to overlap the lower portion of the flight envelope rather than an arbitrary convenient speed, so that at the high end the test reaches genuinely flight-relevant Re. Second, the riblet tiles tested in Configuration C will be fabricated in a matched set of spacings bracketing the predicted optimal s^+ at the actual measured test-section conditions, so that the drag-reduction optimum is located empirically rather than assumed. Third, where full-scale flight Re cannot be reached, boundary-layer transition will be characterized (via the hot-wire traverse and surface-flow visualization) so that the transition location is known and the data can be reported against transition state rather than naively extrapolated. We explicitly do not claim that sub-flight-Re riblet or tubercle performance transfers unchanged to flight; quantifying the Re-sensitivity is itself a stated deliverable.

5.3b Tunnel Selection, Blockage, and Wall Corrections

The deployed Apex arm-to-arm span is approximately 2,450 mm, which is large relative to most academic closed-section tunnels. Solid and wake blockage must be held within correctable limits. The isolated-panel configuration (350 mm chord × 600 mm span) presents modest frontal area and is the primary quantitative configuration for this reason. The full-suit mannequin configuration requires either a large test section (working section minimum span on the order of 2 m for blockage below ≈10°percent at high angle of attack) or a reduced-scale mannequin with the attendant Re penalty noted above. We propose to confirm the host tunnel's working-section dimensions during scoping and to compute the projected solid-, wake-, and (at high AoA) separation-blockage corrections explicitly before committing to full-suit testing; if blockage cannot be held within standard correctable bounds, the full-suit configuration will be descoped to the isolated panel plus a half-model or reduced-span representation.

5.3c Aeroelastic Deformation Measurement

The DragonSuit is, by design, an aeroelastic structure: the SMP rib, the auxetic panel, and the washout weave all deform under aerodynamic load, and that deformation is the mechanism of action rather than a parasitic error. A force balance alone cannot distinguish a wing that is performing as intended from one that has deformed into an unintended shape. The program therefore pairs every force measurement with simultaneous full-field deformation measurement by stereo digital image correlation (stereo-DIC) or photogrammetry on a speckled panel surface, resolving the as-loaded camber, twist distribution, and tip-slot opening at each test condition. This converts each polar point into a measured (shape, force) pair and allows the auxetic camber response and the 3–5° washout target to be validated directly against the loaded geometry rather than inferred.

5.3d Shape-Memory Polymer Thermal State Control

The DiAPLEX SMP rib holds its rigid, geometry-maintaining state below its ≈37°C transition and relaxes above it. In flight the rib is warmed by body contact; in a wind tunnel with no occupant and forced convection at 30–80 m/s, an uncontrolled rib would sit at ambient and its modulus would depend on tunnel temperature. To test the rib in its intended deployed state, the test article incorporates a controlled resistive heating layer maintaining the rib substrate at its specified operating temperature, with embedded thermocouples logging rib temperature throughout each run. Rib thermal state is thus a controlled variable, not an uncontrolled one, and the polar can additionally be measured across the transition to characterize the performance penalty of thermal loss — directly relevant to cold-altitude operation.

5.4 Instrumentation

The following instrumentation suite is proposed. Final instrument specification will be confirmed in coordination with the host aerodynamics laboratory during the project scoping phase.

Instrument	Measurement	Target Accuracy
6-component sting balance (full suit)	CL, CD, CY, Cl, Cm, Cn	±0.2% full scale
2-component force balance (isolated panel)	L, D forces	±0.1% full scale
Surface pressure taps (48–96 locations)	Cp distribution, chordwise and spanwise	±0.05 Cp
Particle Image Velocimetry (PIV)	Velocity field: leading-edge separation, tip vortex structure	Spatial resolution ~1 mm per vector
Tuft visualization	Surface flow attachment/separation topology	Qualitative
Hot-wire anemometry	Boundary layer profiles at 3 chordwise stations	u'/U < 0.5%
Riblet film drag balance (Config C)	Direct skin friction measurement on 150 mm × 150 mm riblet tile vs. smooth reference	±2% of friction force
Stereo digital image correlation (stereo-DIC)	Full-field as-loaded camber, twist distribution, tip-slot opening	±0.1 mm displacement
Embedded thermocouples + resistive heater	SMP rib substrate temperature control and logging	±0.5°C

5.5 Expected Outcomes and Deliverables

The wind tunnel program would deliver:

(1) Experimentally measured CL, CD, and L/D polars for all three test configurations across the full AoA and velocity sweep — the primary validation dataset for the 2× L/D improvement target.

(2) Stall angle characterization as a function of leading-edge tubercle geometry — direct experimental validation of the 22° → 28° stall delay projected from humpback whale fin literature.

(3) Technology contribution matrix from Configuration C isolation testing — per-technology ΔL/D values for comparison with CFD projections in Table 4.1.

(4) PIV flow field data at the leading-edge, mid-chord, and tip vortex planes — the foundation for CFD model validation and future RANS/LES simulation.

(5) A peer-reviewed journal manuscript (target: AIAA Journal or Journal of Fluids and Structures) documenting the experimental methodology, results, and comparison with biomimetic biological data from the primary literature.

6. Anticipated Technical Questions and Risk Register

We have written this section in the voice of the reviewer rather than the proposer. The following are the objections a wind tunnel aerodynamicist should raise on first reading, together with our planned response. We would rather surface them ourselves than have them surface in review.

6.1 "Is this measured at flight Reynolds number, and if not, why should I believe it transfers?"

This is the central question and it is addressed structurally in Sections 5.3a. We do not claim transfer; we claim characterization. The riblet optimum is located empirically at test conditions across a bracketed spacing set, the tubercle effect is reported against measured transition state, and Re-sensitivity is itself a deliverable. Where the high end of the test envelope reaches flight-relevant Re, the data stand directly; where it does not, the data are reported with transition state attached and explicitly not extrapolated.

6.2 "A rigid mannequin L/D is not a flight L/D."

Agreed, and stated in Section 4. The program measures the polar of a defined geometry — a repeatable, physically meaningful quantity — and does not assert it equals the dynamic performance a trained pilot achieves through active body control. The value of the measurement is in the controlled comparison between configurations and against the NACA 4412 baseline, not in a headline flight number.

6.3 "Your wing deforms under load — how do you know its shape during the test?"

Every force measurement is paired with simultaneous stereo-DIC full-field deformation measurement (Section 5.3c). Each polar point is a measured (shape, force) pair. The auxetic camber response and washout twist are validated against the loaded geometry directly rather than assumed from the unloaded CAD.

6.4 "Blockage will dominate a full-suit test in an academic tunnel."

Acknowledged in Section 5.3b. The isolated panel is the primary quantitative configuration precisely because its blockage is modest. Full-suit testing proceeds only if the host working section keeps blockage within standard correctable bounds; otherwise it is descoped to a half-model or reduced-span representation, with the Reynolds penalty of any scale reduction stated.

6.5 "The SMP will not be in its deployed state in an unoccupied mannequin."

Addressed by active thermal control (Section 5.3d). Rib temperature is a logged, controlled variable, and the transition itself is characterized to quantify the cold-loss penalty.

6.6 "You cannot add lift-drag contributions and discount them 30%."

We no longer do. Section 4.1 reports the per-technology figures as isolated directional estimates only, and states that the integrated polar must be measured because the mechanisms are aerodynamically coupled. The Configuration C isolation tests provide attribution; they do not license linear superposition.

6.7 "What about unsteady effects, stall hysteresis, and dynamic stall?"

The proposed program characterizes the static polar, including the post-stall regime, in 1° increments through and beyond stall. Stall hysteresis will be captured by running the angle-of-attack sweep in both increasing and decreasing directions at selected speeds. Genuine dynamic-stall and gust-response characterization is identified as Phase II work requiring a pitching rig and is explicitly out of scope for the initial static program — flagged here so the boundary is clear rather than implied.

6.8 "What is your uncertainty budget?"

Each reported coefficient will carry a propagated uncertainty combining balance accuracy (Section 5.4), dynamic-pressure measurement, model-attitude setting, and blockage-correction uncertainty, reported as error bars on every polar. Repeat runs at a reference condition establish run-to-run repeatability. No performance claim will be reported without its associated uncertainty.

7. Engineering Drawing Package

The following drawings define the test article geometry for wind tunnel fabrication. All dimensions in millimeters unless noted. Reference pilot for full-suit configurations: 5'11" / 150 lb (180 cm / 68 kg). All airfoil profiles reference NACA 4412 series geometry (NACA Report 460, 1935).

Drawing DS-01/12 — Three-View Orthographic, Full Suit

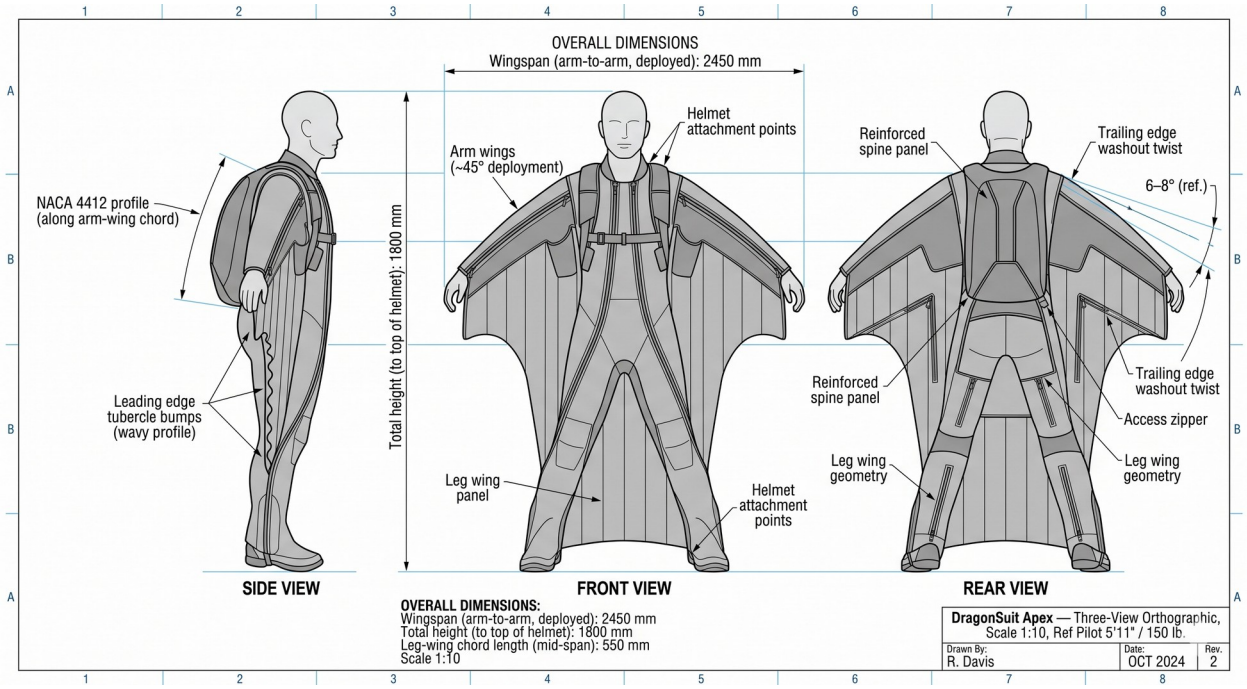

DS-12 — DragonSuit Apex three-view orthographic. Front, side, and rear views at Scale 1:10. Overall dimensions: wingspan arm-to-arm (deployed) 2,450 mm; total height (to helmet top) 1,800 mm; leg-wing chord at mid-span 550 mm. NACA 4412 profile visible along arm-wing chord in side view. Trailing-edge washout twist 6–8° labeled in rear view.

Drawing DS-02 — NACA 4412 Arm-Wing Cross-Section

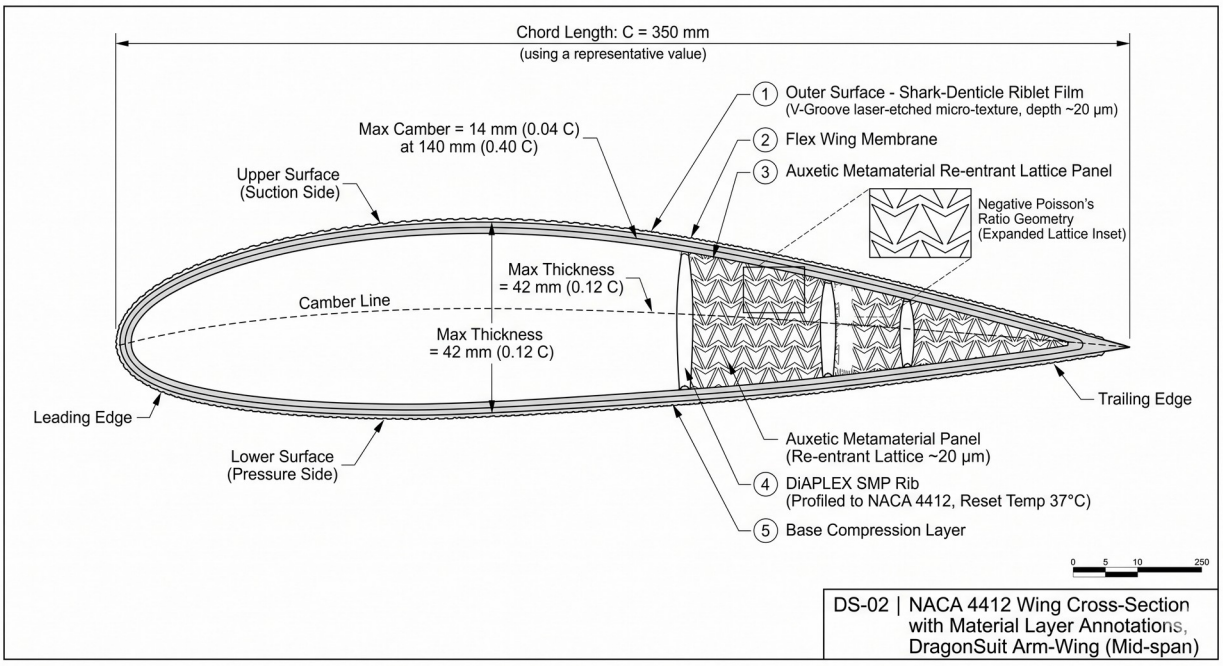

DS-02 — NACA 4412 arm-wing cross-section, mid-span. Chord C = 350 mm. Max camber = 14 mm (4.0% C) at 140 mm (40.0% C). Max thickness = 42 mm (12.0% C). All five composite layers annotated at aft cutaway.

Drawing DS-03 — Five-Layer Stack, Exploded Axonometric

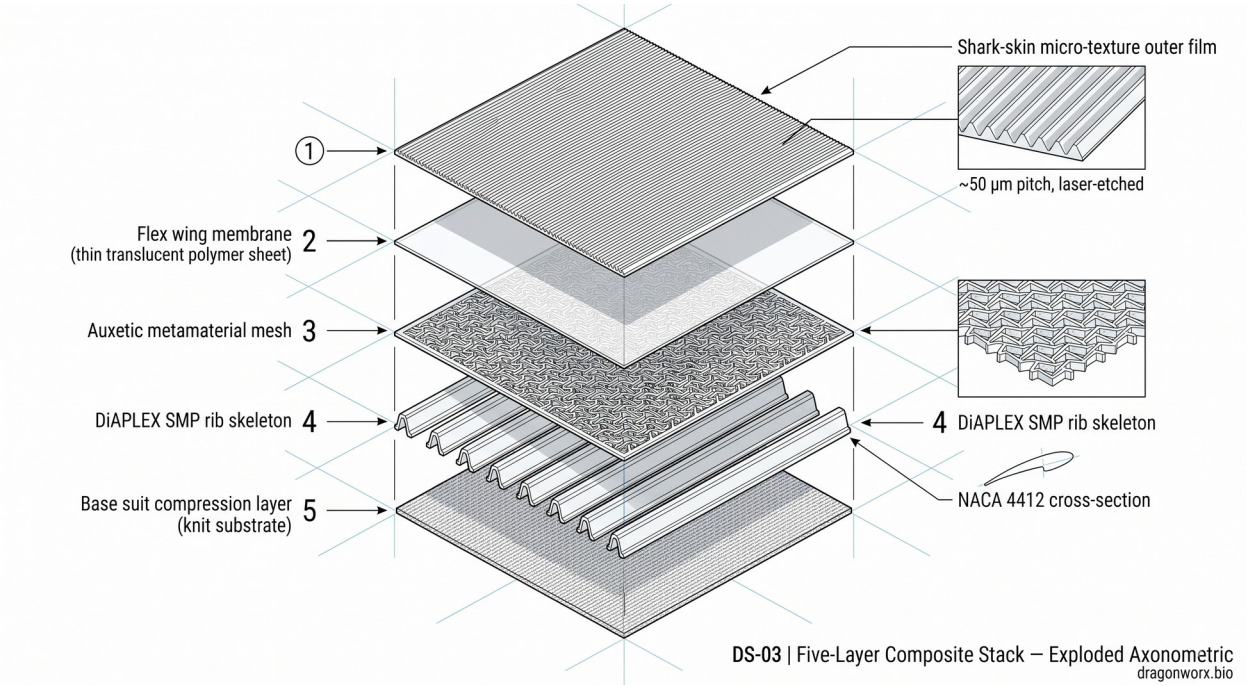

DS-03 — Five-layer composite stack, exploded axonometric. 30 cm × 30 cm representative panel section. Layer separations drawn to approximately 15 mm gap for clarity. Riblet film inset: V-groove cross-section at 500× scale. Auxetic mesh inset: re-entrant hexagonal unit cell at 5× scale.

Drawing DS-05 — Auxetic Metamaterial Panel

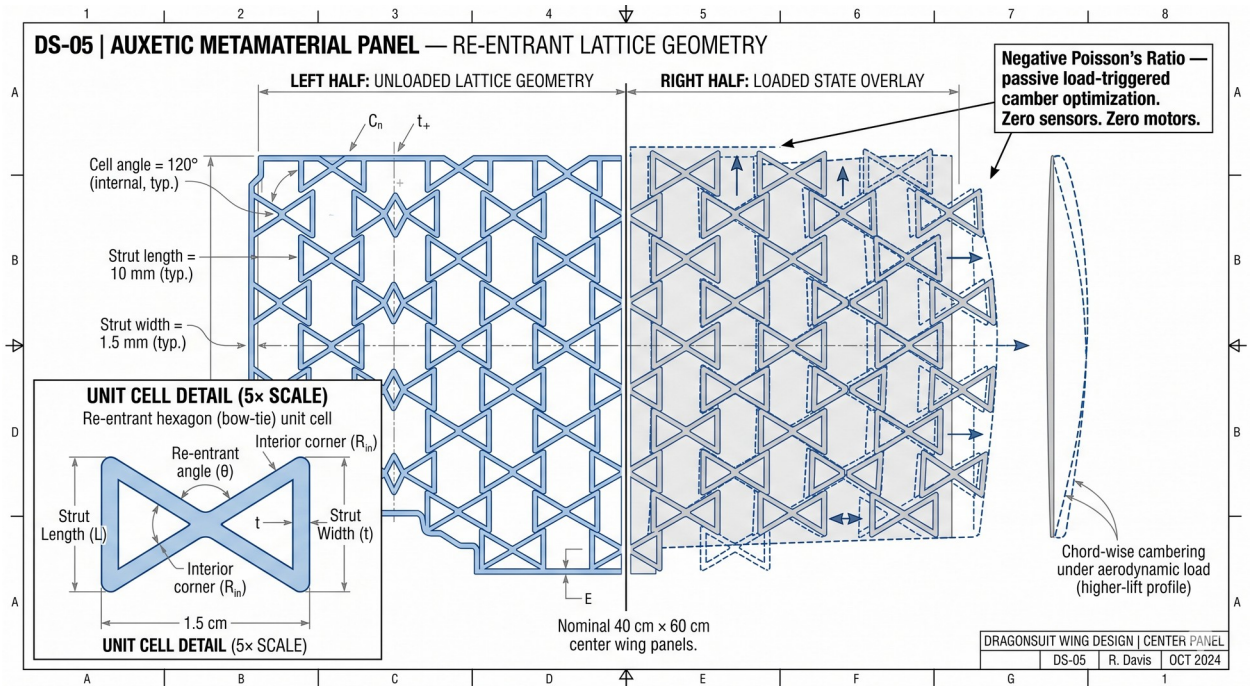

DS-05 — Auxetic metamaterial center wing panel. Nominal dimensions 40 cm × 60 cm. Left: unloaded lattice geometry. Right: loaded state overlay showing expansion under aerodynamic load and chord-wise cambering. Unit cell detail: re-entrant hexagon, L = 10 mm, t = 1.5 mm, θ = 120°. Chord-wise cambering inset at right margin.

Drawing DS-06 — Anisotropic Washout Weave

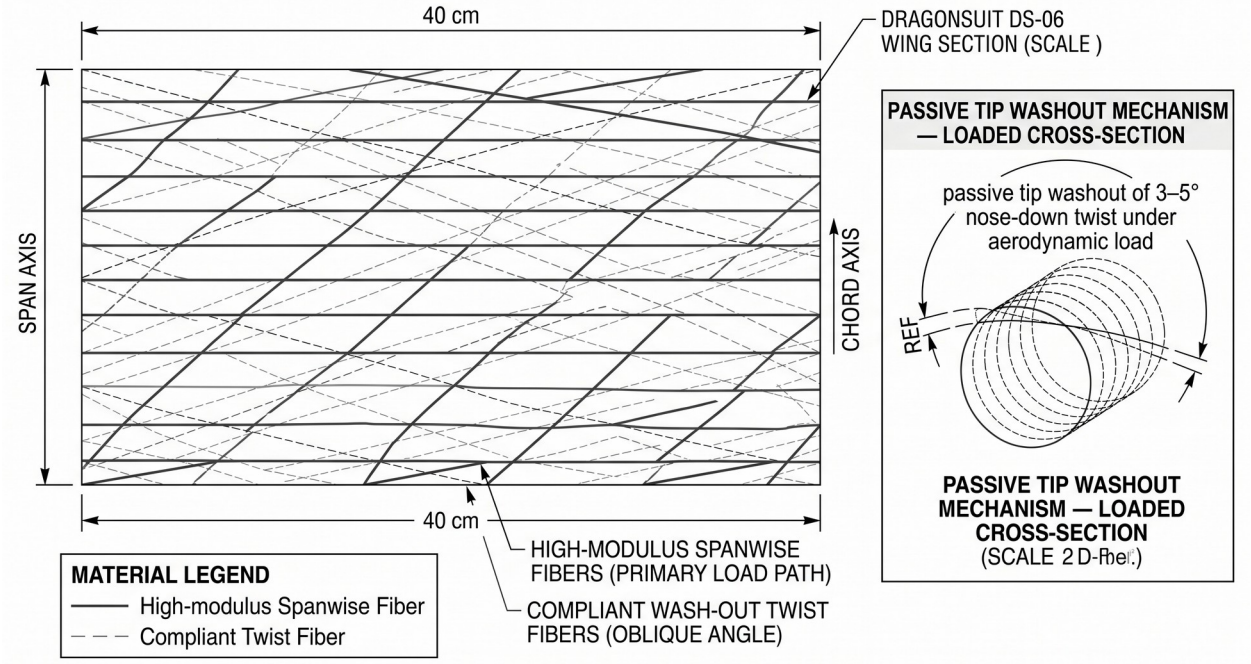

DS-06 — Anisotropic washout weave. 40 cm × 40 cm sample panel. Primary spanwise load-path fibers (solid) and compliant oblique twist fibers (dashed) annotated. Passive tip washout cross-section inset: 3–5° nose-down twist under aerodynamic load.

Drawing DS-07 — Peregrine Tip Slot, Auxetic Wingtip Detail

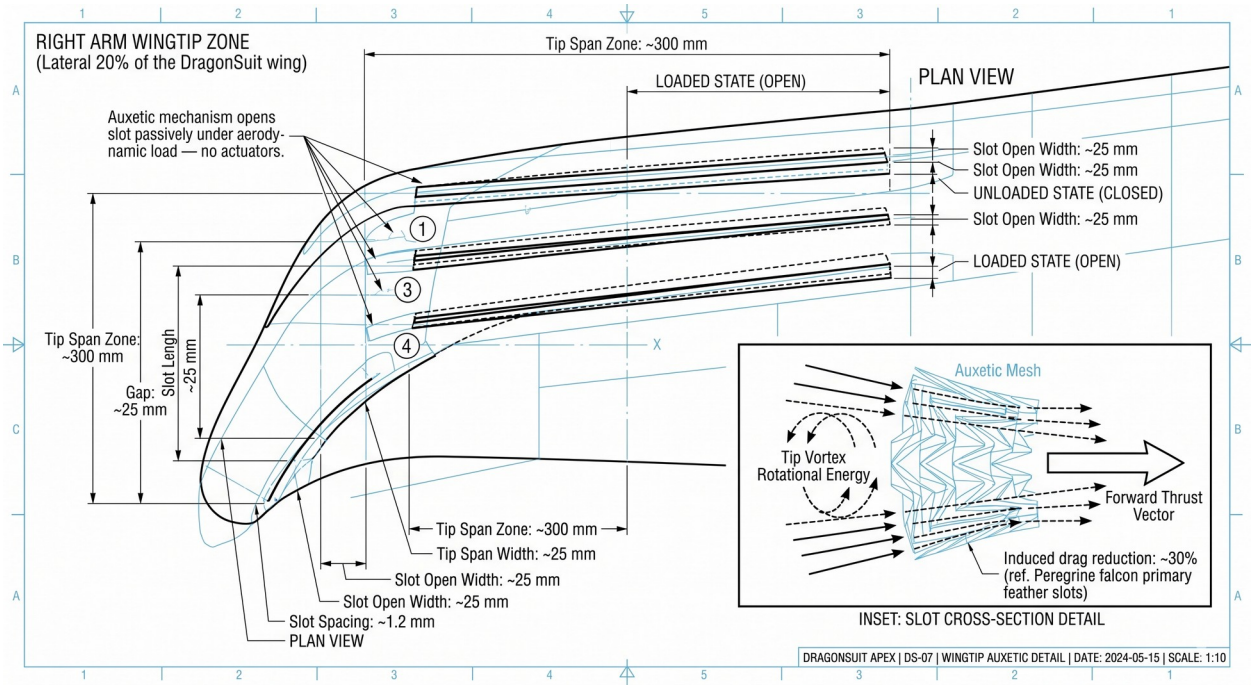

DS-07 — Right arm-wing tip zone (lateral 20% of span, ~300 mm). Four slot gaps, unloaded (closed) and loaded (open) states. Slot open width ~25 mm, slot spacing ~25 mm. Inset: tip vortex rotational energy conversion to forward thrust vector through slotted auxetic mesh. Induced drag reduction target: ~30%.

Drawing DS-08 — Shark-Denticle Riblet Film

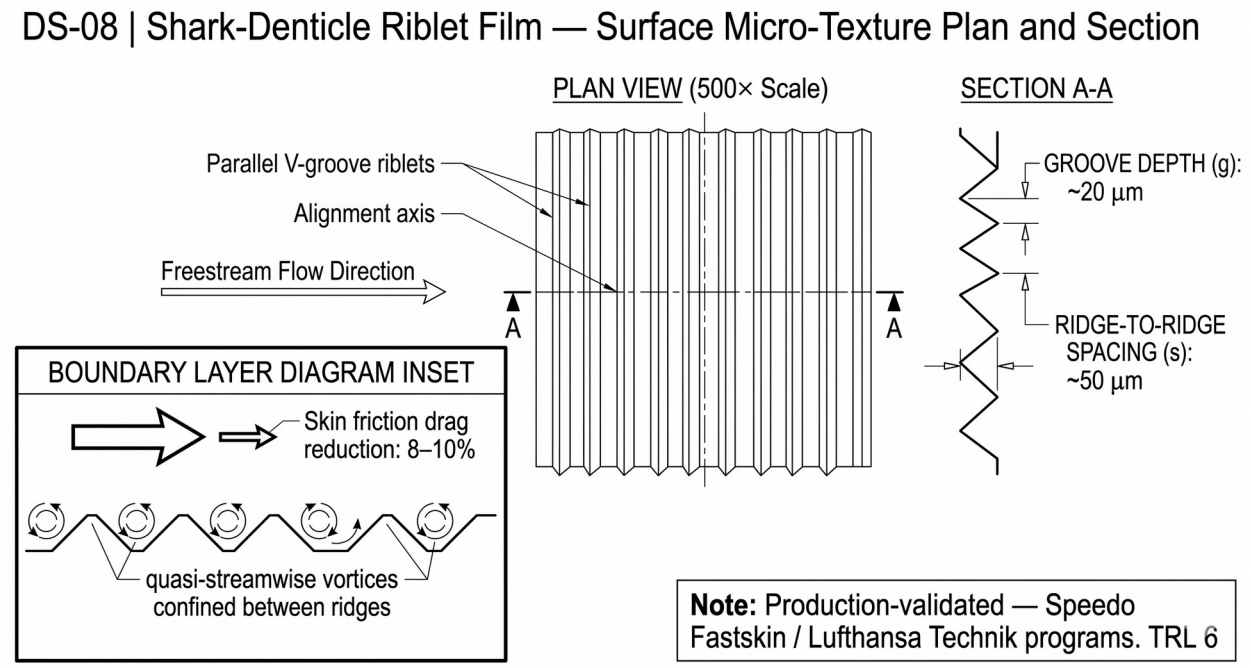

DS-08 — Shark-denticle riblet film surface micro-texture. Plan view at 500× scale: parallel V-groove riblets aligned with freestream direction. Section A-A: groove depth g ≈ 20 µm, ridge-to-ridge spacing s ≈ 50 µm. Boundary layer diagram: quasi-streamwise vortex confinement mechanism. TRL 6, production-validated.

Drawing DS-09 — DiAPLEX SMP Rib Profile

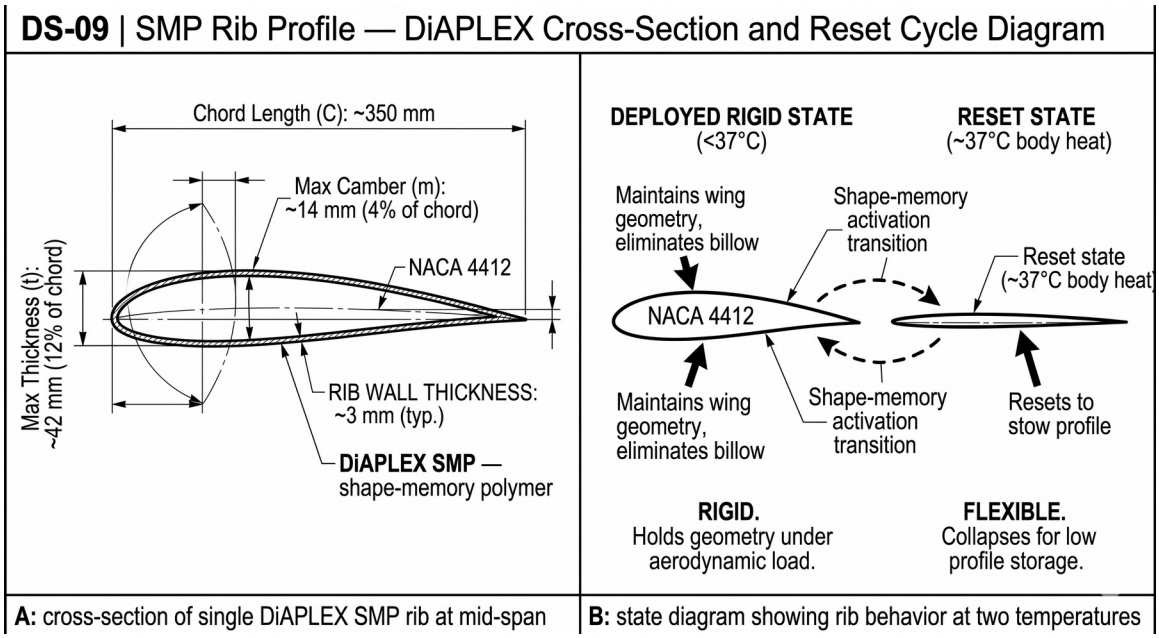

DS-09 — DiAPLEX SMP rib profile and thermal state diagram. Left: NACA 4412 cross-section, C = 350 mm, wall thickness ~3 mm. Right: two-state cycle — glassy (<37°C, rigid, holds geometry) and rubbery (~37°C, flexible, stow profile). Reversible thermal activation.

8. Technology Readiness and Development Roadmap

7.1 TRL Matrix

Technology	Current TRL	Key Evidence	Next Milestone	TRL to Advance
Shark Riblet Film	6	Speedo Fastskin; Lufthansa Technik production validation	Wind tunnel confirmation of 8–10% Cf reduction on DragonSuit panel geometry	7
DiAPLEX SMP Ribs	4	DiAPLEX material TRL; NACA 4412 molding feasibility	Wing tunnel test: SMP rib panel vs. foam rib baseline; L/D comparison	5
Auxetic Metamaterial Panel	4	NPR auxetic structures in published literature; academic prototypes	WT measurement of passive camber response vs. q; PIV confirmation	5
Tubercle Leading Edge	4	Fish et al. wind tunnel data; multiple academic WT studies	WT stall angle measurement on DragonSuit geometry with/without tubercles	5
Peregrine Tip Slot	3	Tucker 1993 avian WT data; auxetic mechanism TRL 4	WT induced drag measurement: slotted vs. closed tip configuration	4
Anisotropic Washout Weave	4–5	Classical composite aeroelastic theory; published washout WT studies	WT twist measurement under load; stall characterization	5
Full Integrated Stack	3–4	Individual technology TRL; CFD integration study	Full-suit WT program (proposed)	5

7.2 Development Timeline

Phase	Duration	Activities	Milestone
Phase 0 — Pre-Test	3 months	Test article fabrication; instrumentation calibration; CFD model finalization	Test article delivery to host facility
Phase 1 — Isolated Panel WT	4 weeks	Config A and C testing; polar measurement; technology isolation	CL/CD polars; technology contribution matrix
Phase 2 — Full Suit WT	4 weeks	Config B testing; full-suit polars; PIV flow field	Full-suit L/D validation; flow field data
Phase 3 — Analysis	3 months	Data reduction; CFD comparison; error analysis	Technical report; journal manuscript submission

Phase 4 — Design Iteration	6 months	Geometry revision based on WT findings; CFD update	Revised design targets; Phase 2 prototype build

9. References and Supporting Literature

The following publications provide the primary scientific basis for each technology in the DragonSuit Apex composite stack.

Tubercle Leading Edges

Fish, F.E., Battle, J.M. (1995). Hydrodynamic design of the humpback whale flipper. Journal of Morphology, 225(1), 51–60.

Fish, F.E., Howle, L.E., Murray, M.M. (2008). Hydrodynamic flow control in marine mammals. Integrative and Comparative Biology, 48(6), 788–800.

Hansen, K.L., Kelso, R.M., Dally, B.B. (2011). Performance variations of leading-edge tubercles for distinct airfoil profiles. AIAA Journal, 49(1), 185–194.

Johari, H., Henoch, C., Custodio, D., Levshin, A. (2007). Effects of leading-edge protuberances on airfoil performance. AIAA Journal, 45(11), 2634–2642.

Shark Riblet Drag Reduction

Bechert, D.W., Bruse, M., Hage, W., Van der Hoeven, J.G.T., Hoppe, G. (1997). Experiments on drag-reducing surfaces and their optimization with an adjustable geometry. Journal of Fluid Mechanics, 338, 59–87.

Walsh, M.J. (1982). Turbulent boundary layer drag reduction using riblets. AIAA Paper 82-0169.

Walsh, M.J. (1990). Effect of detailed surface geometry on riblet drag reduction performance. Journal of Aircraft, 27(6), 572–573.

Speedo International Ltd. (1996). Fastskin swimwear hydrodynamic performance documentation. Internal technical report, referenced in peer-reviewed commentary.

Auxetic Metamaterials

Evans, K.E., Nkansah, M.A., Hutchinson, I.J., Rogers, S.C. (1991). Molecular network design. Nature, 353, 124.

Alderson, A., Alderson, K.L. (2007). Auxetic materials. Proceedings of the Institution of Mechanical Engineers, Part G: Journal of Aerospace Engineering, 221(4), 565–575.

Scarpa, F., Lombardi, M., Chirima, G. (2004). Analysis of the first strain gradient effects on auxetic sandwich structures. Applied Mechanics and Materials, 5–6, 347–354.

Shape-Memory Polymers

Lendlein, A., Kelch, S. (2002). Shape-memory polymers. Angewandte Chemie International Edition, 41(12), 2034–2057.

Mitsubishi Heavy Industries. DiAPLEX Technical Data Sheet: Thermally induced shape memory polyurethane. Product documentation, MHI Advanced Materials Division.

Tip Slots and Induced Drag

Tucker, V.A. (1993). Gliding birds: reduction of induced drag by wing tip slots between the primary feathers. Journal of Experimental Biology, 180, 285–310.

Withers, P.C. (1981). An aerodynamic analysis of bird wings as fixed aerofoils. Journal of Experimental Biology, 90, 143–162.

Passive Washout and Aeroelastic Tailoring

Weisshaar, T.A. (1987). Aeroelastic tailoring of forward swept composite wings. Journal of Aircraft, 18(8), 669–676.

Shirk, M.H., Hertz, T.J., Weisshaar, T.A. (1986). Aeroelastic tailoring — theory, practice, and promise. Journal of Aircraft, 23(1), 6–18.

DARPA Z-Man Program (Gecko Adhesion, Reference for Platform Context)

Hawkes, E.W., Christensen, D.L., Han, A.K., Jiang, H., Cutkosky, M.R. (2015). Dynamic surface grasping with directional adhesion. IEEE/RSJ International Conference on Intelligent Robots and Systems, 6068–6075.

10. Contact and Next Steps

DragonWorx Biomimetic Technologies welcomes discussions with aerodynamics research faculty and wind tunnel facility directors regarding the scope, timeline, funding structure, and intellectual property framework for a collaborative wind tunnel validation program.

Item	Detail
Company	DragonWorx Biomimetic Technologies
Location	Richardson, Texas
Technical Contact	getdragons@dragonworx.bio
Website	dragonworx.bio
Current Funding Status	Seed round in progress — $1.8M target
Wind Tunnel Program Scope	Proposing joint research agreement with IP co-ownership framework
Proposed Start	Q4 2026 or subject to mutual schedule availability

This document is intended solely for the use of the named recipient. Questions? getdragons@dragonworx.bio